ФИЗИКА АТОМНОГО ЯДРА И ЭЛЕМЕНТАРНЫХ ЧАСТИЦ

Известия Саратовского университета. Новая серия. Серия: Физика. 2023. Т. 23, вып. 2. С. 157–166
Izvestiya of Saratov University. Physics, 2023, vol. 23, iss. 2, pp. 157–166
https://fizika.sgu.ru https://doi.org/10.18500/1817-3020-2023-23-2-157-166, EDN: DNUYIV

Article

Systematics of the Coulomb barrier characteristics resulting from M3Y nucleon-nucleon forces for reactions with heavy ions

I. I. Gontchar[1], **M. V. Chushnyakova**[2]✉, **N. A. Khmyrova**[1]

[1]Omsk State Transport University, 35 Marxa prospect, Omsk 644046, Russia
[2]Omsk State Technical University, 11 Mira prospect, Omsk 644050, Russia

Igor I. Gontchar, vigichar@hotmail.com, https://orcid.org/0000-0002-9306-6441
Maria V. Chushnyakova, maria.chushnyakova@gmail.com, https://orcid.org/0000-0003-0891-3149
Natalya A. Khmyrova, nata_ruban@mail.ru, https://orcid.org/0000-0003-0690-9138

Abstract. In the literature, often the capture cross sections for spherical heavy-ions are calculated by virtue of the characteristics of the s-wave barrier: its energy, radius, and stiffness. We evaluate these quantities systematically within the framework of the double-folding model. For the effective nucleon-nucleon forces, the M3Y Paris forces with zero-range exchange part are used. The strength of this part is modified to fit the barrier energy obtained with the density-dependent finite-range exchange part. For the nucleon density, two options are employed. The first one (V-option) is based on the experimental charge densities. The second one, C-option, comes from the IAEA data base; these densities are calculated within the Hartree-Fock-Bogolubov approach. For both options, the analytical approximations are developed for the barrier energy, radius, and stiffness. The accuracy of these approximations is about 3% for the barrier energy and radius and about 10% for the stiffness. The proposed approximations can be easily used by everyone to estimate the capture cross sections within the parabolic barrier approximation.

Keywords: double-folding model, nucleon densities, characteristics of Coulomb barrier

Acknowledgements: This work was supported by the Foundation for the Advancement of Theoretical Physics and Mathematics "BASIS".

For citation: Gontchar I. I., Chushnyakova M. V., Khmyrova N. A. Systematics of the Coulomb barrier characteristics resulting from M3Y nucleon-nucleon forces for reactions with heavy ions. *Izvestiya of Saratov University. Physics*, 2023, vol. 23, iss. 2, pp. 157–166. https://doi.org/10.18500/1817-3020-2023-23-2-157-166, EDN: DNUYIV

Научная статья
УДК 539.17.01

Систематика параметров кулоновских барьеров, вычисленных с использованием M3Y нуклон-нуклонных сил, в реакциях с тяжёлыми ионами

И. И. Гончар[1], **М. В. Чушнякова**[2]✉, **Н. А. Хмырова**[1]

[1]Омский государственный университет путей сообщения, Россия, 644046, г. Омск, пр. Маркса, д. 35
[2]Омский государственный технический университет, Россия, 644050, г. Омск, пр. Мира, д. 11

Гончар Игорь Иванович, доктор физико-математических наук, профессор кафедры «Физика и химия», vigichar@hotmail.com, https://orcid.org/0000-0002-9306-6441

НАУЧНЫЙ ОТДЕЛ

Чушнякова Мария Владимировна, кандидат физико-математических наук, доцент кафедры «Физика», mvchushnyakova@omgtu.tech, https://orcid.org/0000-0003-0891-3149
Хмырова Наталья Анатольевна, кандидат физико-математических наук, доцент кафедры «Физика и химия», nata_ruban@mail.ru, https://orcid.org/0000-0003-0690-9138

Аннотация. В литературе сечения слияния (захвата в орбитальное движение) для сложных сферических ядер часто вычисляются с помощью характеристик барьера, соответствующего лобовому столкновению: высоты барьера, его радиуса и жёсткости. В настоящей работе мы рассчитываем эти величины систематически в рамках модели двойной свёртки. В качестве эффективного нуклон-нуклонного (NN) взаимодействия используется парижское M3Y взаимодействие с нулевым радиусом обменной части. Её амплитуда варьируется так, чтобы воспроизводить высоту барьера, полученного при использовании обменной части с конечным радиусом взаимодействия и плотностной зависимостью NN-взаимодействия. Для нуклонных плотностей использовано два варианта. Первый (V-опция) основан на экспериментальных зарядовых плотностях. Второй (C-опция) – это протонные и нейтронные плотности, вычисленные с помощью подхода Хартри–Фока–Боголюбова и опубликованные МАГАТЭ. Для обеих опций нами построены аналитические аппроксимации высоты барьера, его радиуса и жёсткости. Точность этой аппроксимации составляет около 3% для высоты барьера и около 10% для жёсткости. Предложенные аппроксимации могут быть полезны всем для быстрой оценки сечений захвата с помощью модели параболического барьера.

Ключевые слова: модель двойной свёртки, нуклонные плотности, параметры кулоновского барьера

Благодарности: Настоящая работа была поддержана грантом Фонда развития теоретической физики и математики «БАЗИС».

Для цитирования: *Гончар И. И., Чушнякова М. В., Хмырова Н. А.* Систематика параметров кулоновских барьеров, вычисленных с использованием M3Y нуклон-нуклонных сил, в реакциях с тяжёлыми ионами // Известия Саратовского университета. Новая серия. Серия: Физика. 2023. Т. 23, вып. 2. С. 157–166. https://doi.org/10.18500/1817-3020-2023-23-2-157-166, EDN: DNUYIV

1. Introduction

Collision of two complex nuclei (heavy ions) resulting in the capture of them into orbital motion is the first step for formation of new superheavy chemical elements and/or isotopes [1–6]. The theoretical cross sections of the capture process are subject of significant uncertainties [6–8]. Often the capture cross sections for spherical colliding nuclei are evaluated as follows [9–12]:

$$\sigma_{th} = \frac{\pi\hbar^2}{2m_R E_{c.m.}} \sum_J (2J+1)\, T_J, \qquad (1)$$

$$T_J = \left\{ 1 + \exp\left[\frac{2\pi\,(B_J - E_{c.m.})}{\hbar\omega_{BJ}} \right] \right\}^{-1}. \qquad (2)$$

Here, $E_{c.m.}$ stands for the collision energy; J is the angular momentum in units of $\hbar$; m_R is the reduced mass of colliding ions; B_J and ω_{BJ} are the Coulomb barrier energy and "frequency", respectively. For the J-dependence of the barrier energy, the following approximation is often applied [10, 13, 14]:

$$B_J = B_0 + \frac{\hbar^2 J^2}{2m_R R_{B0}^2}, \qquad (3)$$

where B_0 and R_{B0} are the s-wave barrier energy and radius, respectively. The J-dependence of ω_{BJ} is usually neglected, so

$$\omega_{BJ} = \sqrt{\frac{-C_{B0}}{m_R}} \qquad (4)$$

where C_{B0} is the second derivative of the nucleus-nucleus potential with respect to the center-to-center distance.

Thus, for the fast evaluation of the capture cross section by means of Eq. (1), it is sufficient to know B_0, R_{B0}, C_{B0}. For finding these quantities, one needs the s-wave nucleus-nucleus potential which consists of the Coulomb $U_C(R)$ and nuclear $U_n(R)$ terms.

The nuclear term (Strong nucleus-nucleus Potential, SnnP) is a crucial ingredient for any theoretical description of the capture process. Often for SnnP they use the Woods–Saxon profile [15–19]. The parameters of this profile (depth, diffuseness, and radius) are varied more or less arbitrary to fit σ_{th} to the above barrier experimental capture cross sections. Obviously, the Woods-Saxon profile represents the SnnP only qualitatively.

The much better founded proximity potential [20, 21] is employed every now and again [22–26]. This potential includes a universal dimensionless function independent of the colliding nuclei. Yet some parameters of this potential can be varied individually for a given reaction.

The single-folding potential [27, 28] is more rigorous. For evaluating this potential one needs to know: (i) the distributions of the nucleon centers of mass (the nucleon densities) for both colliding nuclei; and (ii) the interaction energy between the whole target (projectile) nucleus and a nucleon of the projectile (target) nucleus. For the nucleon densities, the two-parameter Fermi profile was applied in [27–29]. The parameters of the profile might be obtained from the electron scattering data [30]. However, the electron scattering is only sensitive to the Coulomb interaction. Therefore, in such experi-

ments the charge density distribution is measured, not the nucleon density. The direct experimental information of the nucleon density is scares [31–33]. For the second ingredient of the single-folding potential being the nucleon–nucleus potential, usually the Woods–Saxon profiles are used. Parameters of these profiles are extracted from the fit of the elastic scattering data [28]. Thus, the single-folding approach still has six individual fit parameters for a given reaction.

Employing the effective nucleon–nucleon forces (*NN* forces) seems to be the next step towards a more realistic description of the nucleus–nucleus potential. This step is realized in the double-folding (DF) model [34, 35]. The nucleon densities of the colliding nuclei are one more ingredient of this model. Three such DF potentials using different effective *NN* forces are known in the literature: i) with the M3Y ones [36,37]; ii) with the relativistic mean-field ones [8, 38, 39]; iii) with the Migdal forces [40, 41].

The aim of the present work is to calculate systematically the characteristics of the heavy-ion s-wave Coulomb barriers B_0, R_{B0}, C_{B0} obtained within the framework of the DF approach with the M3Y *NN* forces and to explore whether there are any regularities in their behavior versus the approximate barrier energy

$$B_Z = \frac{Z_P Z_T}{A_P^{1/3} + A_T^{1/3}} \text{ MeV}. \qquad (5)$$

The present paper is organized as follows. Section 2 is devoted to the DF model applied for the calculation of the nucleus-nucleus potential. The nucleon densities are discussed in Sec. 3. Sections 4 and 5 represent the results obtained for two sorts of densities. Conclusions are collected in Sec. 6.

2. The double-folding model

The nucleus-nucleus s-wave potential U_0 versus the distance R between the centers of mass of spherical projectile (P) and target (T) nuclei reads

$$U_0(R) = U_C(R) + U_{nD}(R) + U_{nE}(R). \qquad (6)$$

Here U_C is the Coulomb term, U_{nD} and U_{nE} stand for the direct and exchange parts of the SnnP, respectively. These three terms read

$$U_C = \int d\vec{r}_P \int d\vec{r}_T \rho_{qP}(r_P)\, v_C(s)\, \rho_{qT}(r_T), \qquad (7)$$

$$U_{nD} = \int d\vec{r}_P \int d\vec{r}_T \rho_{AP}(r_P)\, v_D(s)\, \rho_{AT}(r_T), \qquad (8)$$

$$U_{nE} = \int d\vec{r}_P \int d\vec{r}_T \rho_{AP}(r_P)\, v_E(s)\, \rho_{AT}(r_T). \qquad (9)$$

Here ρ_{AP} and ρ_{AT} (ρ_{qP} and ρ_{qT}) denote the nucleon (charge) densities, r_P and r_T are the absolute values of the radius-vectors of the interacting points of the projectile and target nuclei. Vector $\vec{s}$ connects two interacting points and is determined by vectors $\vec{R}$, $\vec{r}_P$, and $\vec{r}_T$ (see Fig. 2 in [42, 43] or Fig. 1 in [44, 45]). The point-point Coulomb potential is denoted as $v_C(s)$.

In Eqs. (7), (8), (9), we neglect the possible time-dependence of the densities. This so-called frozen density approximation (FDA) seems to work reasonably well unless the density overlap of the colliding nuclei is about 1/3 of the saturation density 0.16 fm^{-3}. Recently, the FDA was inspected carefully and compared with the adiabatic density approximation (ADA) in Ref. [46].

The direct part of the *NN*-interaction $v_D(s)$ consists of two Yukawa terms [47, 48]:

$$v_D(s) = \sum_{i=1}^{2} G_{Di} \left[\exp\left(\frac{-s}{r_{vi}}\right)\right] / \left(\frac{s}{r_{vi}}\right). \qquad (10)$$

For the exchange part $v_E(s)$, one finds in the literature two options: an advanced and complicated one with a finite range and a simpler one with zero range [42, 48]. Equation (9) is valid for the latter version for which

$$v_E(s) = G_E \delta(\vec{s}). \qquad (11)$$

It has been demonstrated recently [44] that varying the value of G_E with respect to its standard value -592 MeV fm^3 from Ref. [37] down to -1040 MeV fm^3 allows to reproduce the Coulomb barrier energies resulting from the option with the finite range exchange force. Computer calculations with zero-range option are significantly faster than those ones with the finite range option. In the present paper, we apply Eqs. (9), (11) with $G_E = -1040$ MeV fm^3.

+

3. Nucleon densities

In the present study, we employ two prescriptions for the nucleon densities coming from Refs. [30] and [49]. We denote them as V-densities and C-densities, respectively. In both sources [30] and [49], the density is approximated by the three-parameter Fermi formula (3pF-formula)

$$\rho_F(r) = \rho_{0F} \frac{1 - w_F r^2/R_F^2}{1 + \exp[(r - R_F)/a_F]}. \qquad (12)$$

Here R_F corresponds approximately to the half central density radius, a_F is the diffuseness, ρ_{0F} is

defined by a normalization condition. In Ref. [30], the 3pF-formula (or its version with $w_F = 0$ called 2pF-formula) is applied to approximate the experimental charge density (in this case the subscript F takes the value Vq). We use the same 3pF-formulas for proton ($F = Vp$) and neutron ($F = Vn$) densities for a given nucleus. The parameters R_{Vq}, a_{Vq}, and w_{Vq} of the charge density are taken from Ref. [30]. The half-density radii for protons R_{Vp} and neutrons R_{Vn} as well as w_{Vp} and w_{Vn} are taken to be equal to R_{Vq} and w_{Vq}, respectively, whereas the proton and neutron diffusenesses, a_{Vp} and a_{Vn}, are calculated via the charge diffuseness a_{Vq} [42, 43]:

$$a_{Vp} = a_{Vn} = \sqrt{a_{Vq}^2 - \frac{5}{7\pi^2}\left(0.76 - 0.11\frac{N}{Z}\right)}. \quad (13)$$

We use all spherical nuclei for which Eq. (12) is available in Ref. [30]. The values of the parameters are presented in Table 1.

In Ref. [49], theoretical proton and neutron densities calculated within the Hartree–Fock–Bogolubov approach are approximated by Eq. (12) with $w_F = 0$. In this case, the subscript F takes the values Cp, Cn, and Cq. We take $R_{Cq} = R_{Cp}$ and

$$a_{Cq} = \sqrt{a_{Cp}^2 + \frac{5}{7\pi^2}\left(0.76 - 0.11\frac{N}{Z}\right)}. \quad (14)$$

The values of the parameters are again presented in Table 1.

4. Results: V-densities

In Fig. 1, *a*, we present the calculated s-wave Coulomb barrier energies B_{0V}. These calculations are performed for four groups of the reactions induced by: ^{16}O, ^{40}Ca, ^{58}Ni, and ^{88}Sr (symbols). This allows to cover a wide range of $B_Z = 12 \div 300$ MeV. The line in the figure corresponds to $B_0 = B_Z$. One sees that B_Z is indeed a good approximation for the DF M3Y barrier energies.

The fractional difference between these two quantities

$$\xi_B = \frac{B_0}{B_Z} - 1 \quad (15)$$

is displayed in Fig. 1, *b*. The symbols correspond to DF M3Y-calculations where the curve represents

Table 1. Parameters of Eq. (12) for the V- and C-densities for the spherical nuclei involved in the considered reactions. R_{Vq}, w_{Vq}, a_{Vq} of the charge V-densities are taken from Ref. [30] and a_{Vp} for the proton and neutron V-densities calculated according to Eq. (13). R_{Cp}, a_{Cp}, R_{Cn}, a_{Cn} for the proton and neutron C-densities are taken from Ref. [49] and a_{Cq} for the charge C-densities are calculated using Eq. (14)

Nuc.	R_{Vq}, fm	w_{Vq}	a_{Vq}, fm	a_{Vp}, fm	R_{Cp}, fm	a_{Cp}, fm	R_{Cn}, fm	a_{Cn}, fm	a_{Cq}, fm
^{16}O	2.608	−0.051	0.513	0.465	2.699	0.447	2.652	0.460	0.497
^{40}Ar	3.730	−0.190	0.620	0.582	3.657	0.480	3.564	0.532	0.525
^{40}Ca	3.766	−0.161	0.585	0.543	3.564	0.532	3.685	0.481	0.575
^{48}Ca	3.737	−0.030	0.524	0.481	3.887	0.467	3.989	0.493	0.512
^{48}Ti	3.843	0.000	0.588	0.548	3.942	0.477	3.979	0.478	0.523
^{52}Cr	4.010	0.000	0.497	0.449	4.064	0.467	4.085	0.470	0.514
^{54}Fe	4.075	0.000	0.506	0.458	4.145	0.463	4.127	0.463	0.511
^{58}Ni	4.309	−0.131	0.517	0.470	4.241	0.467	4.156	0.512	0.515
^{60}Ni	4.489	−0.267	0.537	0.492	4.274	0.471	4.128	0.532	0.518
^{62}Ni	4.443	−0.209	0.537	0.495	4.318	0.468	4.177	0.532	0.514
^{64}Ni	4.212	0.000	0.578	0.538	4.362	0.465	4.298	0.567	0.511
^{88}Sr	4.830	0.000	0.449	0.496	4.911	0.480	4.971	0.488	0.525
^{112}Sn	5.375	0.000	0.560	0.518	5.404	0.463	5.331	0.555	0.509
^{116}Sn	5.358	0.000	0.550	0.508	5.458	0.459	5.396	0.568	0.505
^{118}Sn	5.412	0.000	0.560	0.519	5.484	0.457	5.428	0.574	0.503
^{120}Sn	5.315	0.000	0.576	0.537	5.508	0.455	5.458	0.546	0.501
^{124}Sn	5.490	0.000	0.534	0.492	5.556	0.452	5.570	0.552	0.497
^{142}Nd	5.774	0.000	0.513	0.468	5.872	0.466	5.865	0.534	0.511
^{148}Sm	5.771	0.000	0.596	0.558	5.9548	0.4721	5.9360	0.5575	0.517
^{206}Pb	6.610	0.000	0.545	0.504	6.6800	0.4666	6.6999	0.5542	0.511

the following approximation

$$\xi_{BV} = 0.106 - 0.219 \cdot \exp\left(\frac{-B_Z}{16.1\ \text{MeV}}\right) - \\ -0.230 \cdot \exp\left(\frac{-B_Z}{206\ \text{MeV}}\right). \quad (16)$$

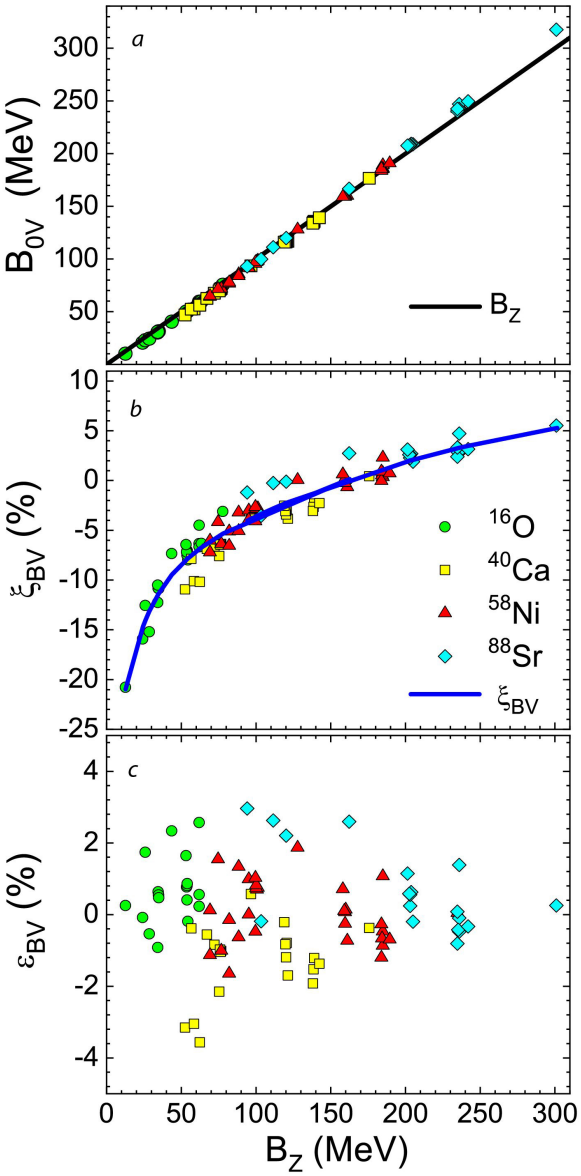

Fig. 1. (*a*) Calculated s-wave Coulomb barrier energies B_{0V}, (*b*) fractional barrier differences ξ_B (see Eq. (15)), and (*c*) errors ε_{BV} (see Eq. (17)) are shown as functions of the approximate barrier energy B_Z for four groups of the reactions induced by: ^{16}O, ^{40}Ca, ^{58}Ni, and ^{88}Sr (symbols). The line in panel (*a*) corresponds to $B_0 = B_Z$, the line in panel (*b*) is the approximation (see Eq. (16)) (color online)

Thus, employing Eqs. (5), (15), (16) one obtains the value of B_0 with the typical accuracy of 1–2% (see Fig. 1, *c*). We define the error of approximation for quantity x as

$$\varepsilon_x = \frac{x_{fit}}{x_{calc}} - 1. \quad (17)$$

Let us go over to the stiffness of the barrier, C_{B0}. The calculated values are shown by symbols in Fig. 2, *a*, their linear fit reads

$$C_{B0V} = -0.755\ \text{MeV} - 0.0494 B_Z \quad (18)$$

(line in Fig. 2, *a*). Accuracy of this fit is typically within 10% (see Fig. 2, *b*) although for lighter reactions it reaches −20% due to smaller values of the stiffness.

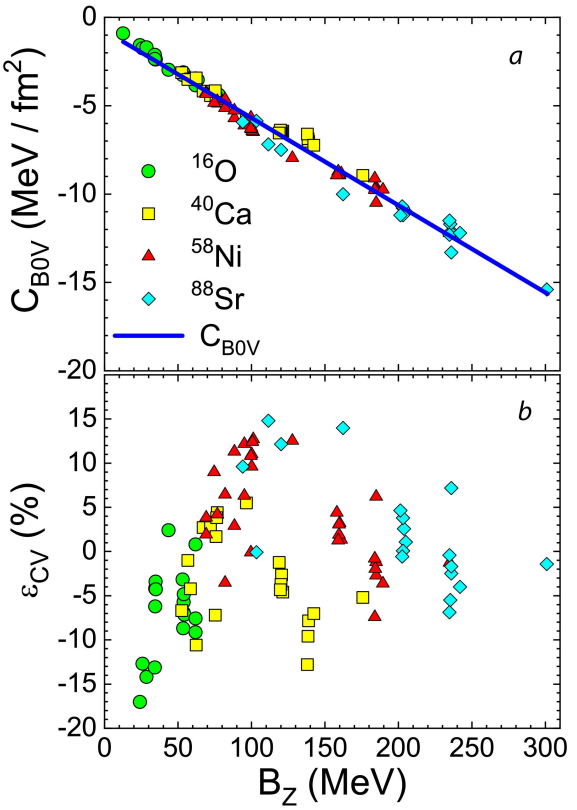

Fig. 2. (*a*) Barrier curvatures C_{B0V} and (*b*) errors ε_{CV} (see Eq. (17)) are shown as functions of B_Z for four groups of the reactions (symbols). The line in panel (*a*) is the approximation (see Eq. (18)) (color online)

The calculated barrier radii versus B_Z are shown by symbols in Fig. 3, *a*. However, their dependence upon $A_P^{1/3} + A_T^{1/3}$ is simpler and more regular (see Fig. 3, *b*). The linear fit of this dependence reads

$$R_{B0V}/\text{fm} = 3.89 + 0.918\left(A_P^{1/3} + A_T^{1/3}\right) \quad (19)$$

(line in Fig. 3, *b*). Typical error of this fit is within 2% (see Fig. 3, *c*).

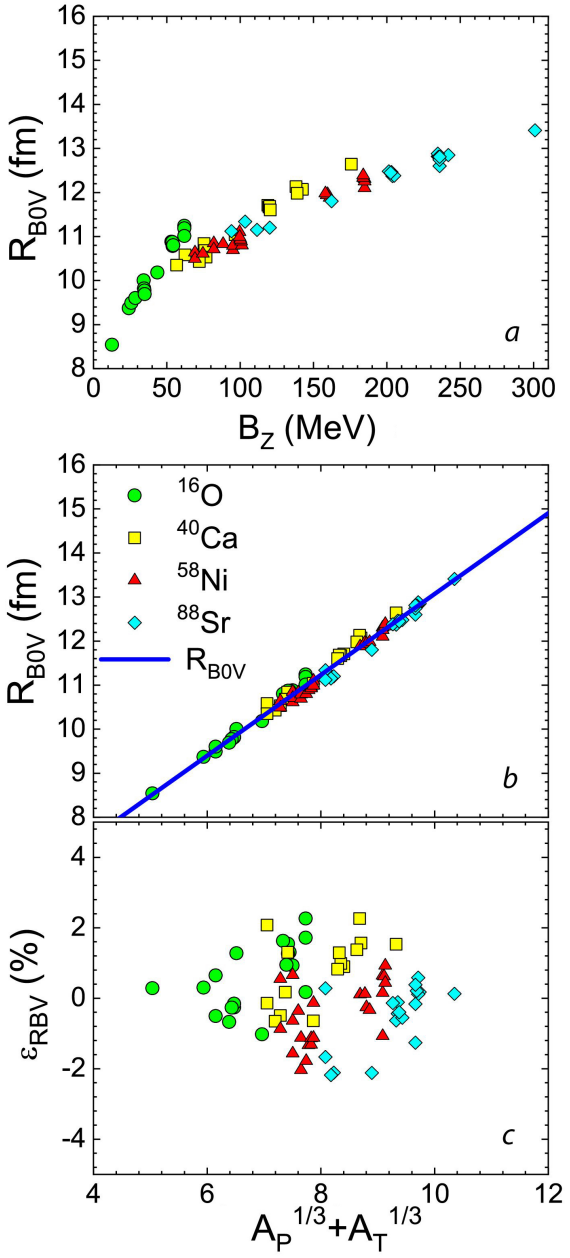

Fig. 3. (*a*) Barrier radii R_{B0V} as functions of B_Z, (*b*) the same R_{B0V} and (*c*) errors ε_{RV} (see Eq. (17)) versus $A_P^{1/3}+A_T^{1/3}$ are shown for four groups of the reactions (symbols). The line in panel (*b*) is the approximation (see Eq. (19)) (color online)

5. Results: C-densities

The same procedure, as in Sec. 4, was performed for C-densities. Results are shown in Figs. 4–6. The approximate formulas read

$$\xi_{BC} = 0.0591 - 0.212 \cdot \exp\left(\frac{-B_Z}{16.1\ \text{MeV}}\right) - \\ -0.197 \cdot \exp\left(\frac{-B_Z}{155\ \text{MeV}}\right), \qquad (20)$$

$$C_{B0C} = -0.752\ \text{MeV} - 0.04648 B_Z, \qquad (21)$$

$$R_{B0C}/\text{fm} = 3.80 + 0.95\left(A_P^{1/3} + A_T^{1/3}\right) \qquad (22)$$

The quality of the fits is approximately as for the case of V-densities (see Figs. 4, *c*, 5, *c*, 6, *c*).

These three approximations for the characteristics of the s-wave Coulomb barrier obtained for V- and C-densities are compared in Fig. 7. Obviously, the trends for two versions of densities coincide with each other in all three panels. As reactions become heavier, the difference appears to be more significant. Although the pairs of curves are close to each other in Fig. 7, one should remember that several percent difference in the barrier energy might influence the fusion cross section substantially, especially for the near- and sub-barrier energies.

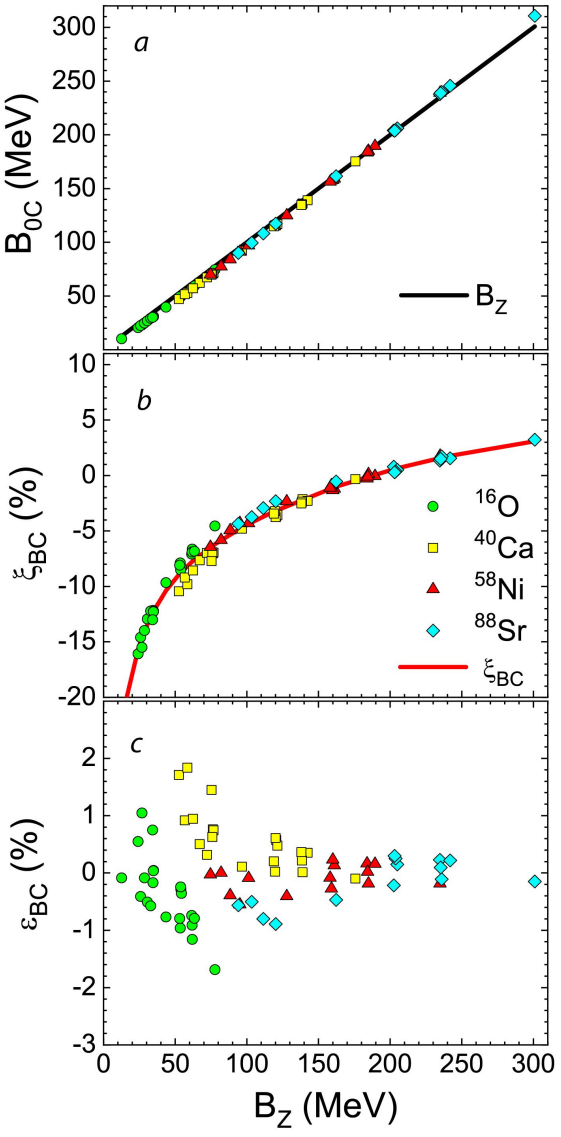

Fig. 4. Same as in Fig. 1 but for C-densities. The line in panel (*b*) corresponds to Eq. (20) (color online)

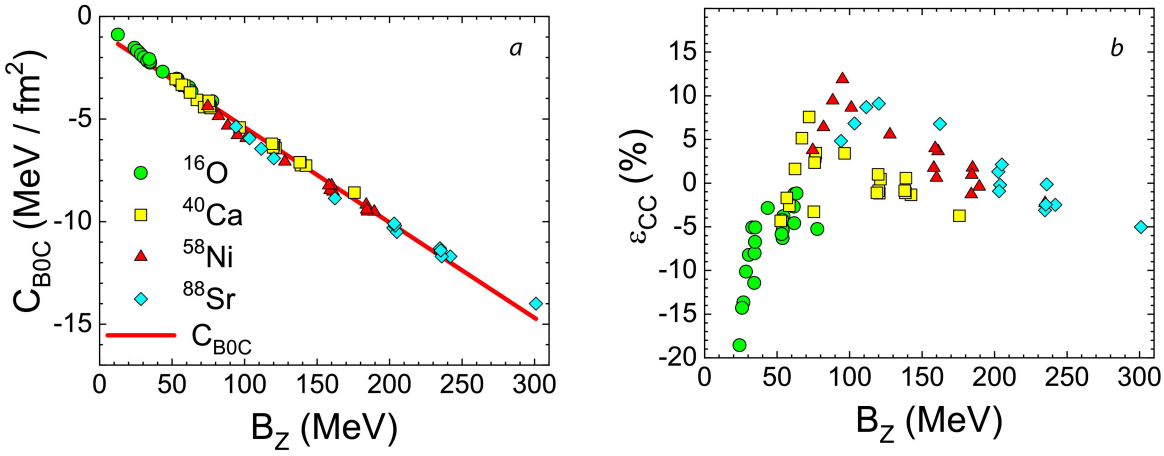

Fig. 5. Same as in Fig. 2 but for C-densities. The line in panel (*a*) corresponds to Eq. (21) (color online)

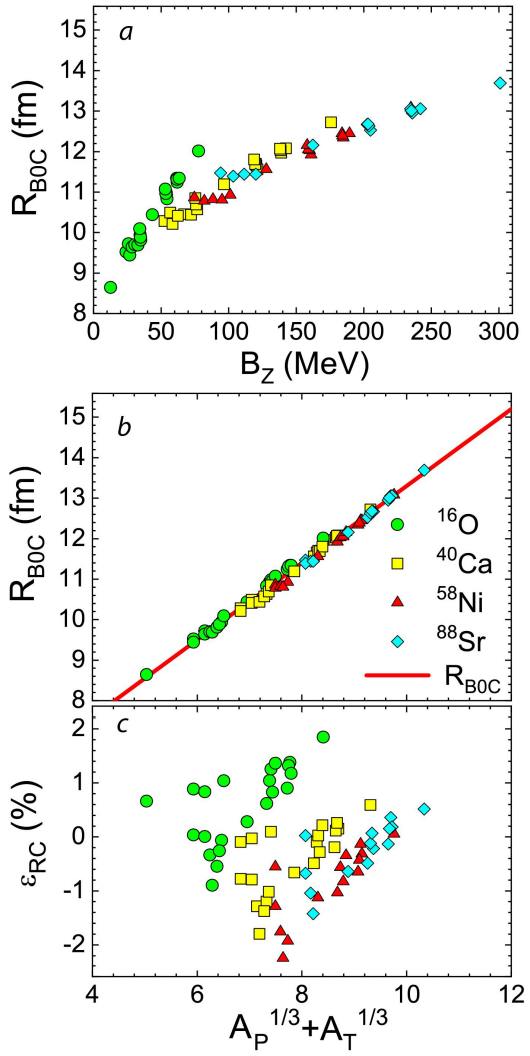

Fig. 6. Same as in Fig. 3 but for C-densities. The line in panel (*b*) corresponds to Eq. (22) (color online)

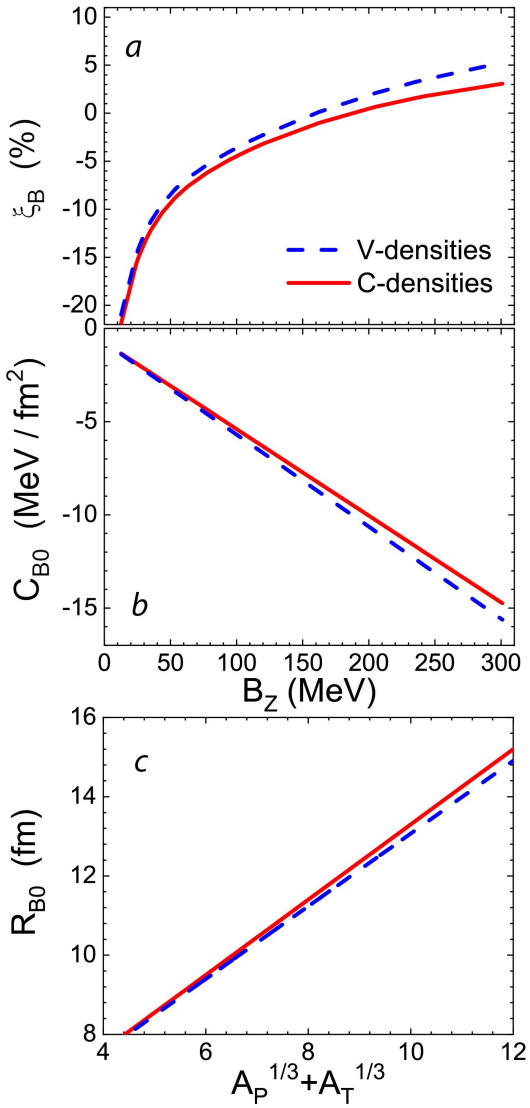

Fig. 7. Comparison between the approximations for the barrier characteristics obtained with V- and C-densities: (*a*) barrier energies B_0 (see Eqs. (16) and (20)), (*b*) barrier curvatures C_{B0} (see Eqs. (18) and (21)), and (*c*) barrier radii R_{B0} (see Eqs. (19) and (22)) (color online)

6. Conclusions

In the literature, every now and again, the spherical heavy-ion capture cross sections are evaluated using the characteristics of the s-wave barrier: its energy, radius, and stiffness. In the present work, we have calculated these quantities systematically within the framework of the double-folding (DF) model. In these calculations, for the effective nucleon-nucleon forces the M3Y Paris forces with zero-range exchange part have been used. The amplitude of this part has been modified to reproduce the barrier energy obtained with the density-dependent finite-range exchange part. For the nucleon density, two options have been used. The first one (V-option) is based on the experimental charge densities. The second one (C-option) has come from the IAEA data base.

For both options, the analytical approximations have been obtained for three quantities required for evaluation of the capture cross sections within the barrier penetration model (parabolic barrier approximation). The comparison of the V- and C-approximations demonstrates that those are not very different. The proposed approximations can be used by everyone for fast estimation of the capture cross sections in the collision of two spherical complex nuclei.

We would like to stress that in the literature there are many recipes for crucial ingredients of the DF model, namely the effective NN-forces and nucleon densities. For instance, in the literature sometimes the Reid M3Y forces [36] are used although in Ref. [37] it is clearly stated that "The Reid soft-core potential is based on earlier and partially erroneous phase-shift data". The Migdal forces were used successfully in quantum diffusion model [41, 50, 51], however for this aim very special nucleon densities were employed. Application of the Migdal forces with densities coming from the Hartree-Fock SKX calculations [52] results in cross sections which do not leave any room for dissipation of collective energy [53]. We believe that the versions of NN-forces and densities used in the present work are the best which are available in the literature for systematic calculations. At the time being, we do not see any arguments allowing to prefer C- or V-option of the densities.

Of course, one would like to see an application of the proposed approximation for the analysis of experimental cross sections as well as a numerical analysis of the accuracy of approximate formulas (3) and (4). However, this would make the present paper unjustifiably long and would distract the attention of the reader. We hope to complete such study in near future.

References

1. Hofmann S., Münzenberg G. The discovery of the heaviest elements. *Rev. Mod. Phys.*, 2000, vol. 72, pp. 733–767. https://doi.org/10.1103/RevModPhys.72.733
2. Berriman A. C., Hinde D. J., Dasgupta M., Morton C. R., Butt R. D., Newton J. O. Unexpected inhibition of fusion in nucleus–nucleus collisions. *Nature*, 2001, vol. 413, pp. 144–147. https://doi.org/10.1038/35093069
3. Oganessian Yu. Ts., Utyonkov V. K. Superheavy nuclei from ^{48}Ca-induced reactions. *Nucl. Phys. A*, 2015, vol. 944, pp. 62–98. https://doi.org/10.1016/j.nuclphysa.2015.07.003
4. Andreyev A. N., Antalic S., Ackermann D., Cocolios T. E., Comas V. F., Elseviers J., Franchoo S., Heinz S., Heredia J. A., Heßberger F. P., Hofmann S., Huyse M., Khuyagbaatar J., Kojouharov I., Kindler B., Lommel B., Mann R., Page R. D., Rinta-Antilla S., Sapple P. J., Šáro Š., Duppen P. Van, Venhart M., Watkins H. V. α decay of ^{180,181}Pb. *Phys. Rev. C*, 2009, vol. 80, article no. 054322. https://doi.org/10.1103/PhysRevC.80.054322
5. Kalaninová Z., Andreyev A. N., Antalic S., Heßberger F. P., Ackermann D., Andel B., Drummond M. C., Hofmann S., Huyse M., Kindler B., Lane J. F. W., Liberati V., Lommel B., Page R. D., Rapisarda E., Sandhu K., Šáro Š., Thornthwaite A., Duppen P. Van. α decay of the very neutron-deficient isotopes $^{197-199}$Fr. *Phys. Rev. C*, 2013, vol. 87, article no. 044335. https://doi.org/10.1103/PhysRevC.87.044335
6. Loveland W. An experimentalist's view of the uncertainties in understanding heavy element synthesis. *Eur. Phys. J. A*, 2015, vol. 51, article no. 120. https://doi.org/10.1140/epja/i2015-15120-2
7. Newton J. O., Butt R. D., Dasgupta M., Hinde D. J., Gontchar I. I., Morton C. R., Hagino K. Systematics of precise nuclear fusion cross sections: The need for a new dynamical treatment of fusion? *Phys. Lett.*, 2004, vol. B586, pp. 219–224. https://doi.org/10.1016/j.physletb.2004.02.052
8. Chushnyakova M. V., Gontchar I. I., Khmyrova N. A. Detail study of application of the relativistic mean-field effective NN forces for heavy-ion fusion within a dynamical model. *J. Phys.*, 2021, vol. G48, article no. 015101. https://doi.org/10.1088/1361-6471/ab907a
9. Fröbrich P., Lipperheide R. *Theory of nuclear reactions*. Clarendon Press, Oxford, 1996. 476 p.
10. Ismail M., Ramadan K. A. Microscopic calculation of sub-barrier fusion cross section and barrier distribution using M3Y-type forces. *J. Phys.*, 2000, vol. G26, pp. 1621–1633. https://doi.org/10.1088/0954-3899/26/10/312
11. Zagrebaev V. I., Aritomo Y., Itkis M. G., Oganessian Yu. Ts., Ohta M. Synthesis of superheavy nuclei:

How accurately can we describe it and calculate the cross sections? *Phys. Rev.*, 2001, vol. C65, article no. 014607. https://doi.org/10.1103/PhysRevC.65.014607

12. Chushnyakova M. V., Gontchar I. I. Oscillations of the fusion cross-sections in the $^{16}O+^{16}O$ reaction. *Pramana*, 2015, vol. 85, pp. 653–665. https://doi.org/10.1007/s12043-014-0917-0
13. Wong C. Y. Interaction Barrier in Charged-Particle Nuclear Reactions. *Phys. Rev. Lett.*, 1973, vol. 31, pp. 766–769. https://doi.org/10.1103/PhysRevLett.31.766
14. Glas D., Mosel U. Limitation on complete fusion during heavy-ion collisions. *Phys. Rev.*, 1974, vol. C10, pp. 2620–2622. https://doi.org/10.1103/PhysRevC.10.2620
15. Leigh J. R., Dasgupta M., Hinde D. J., Mein J. C., Morton C. R., Lemmon R. C., Lestone J. P., Newton J. O., Timmers H., Wei J. X., Rowley N. Barrier distributions from the fusion of oxygen ions with $^{144,148,154}Sm$ and ^{186}W. *Phys. Rev.*, 1995, vol. C52, pp. 3151–3166. https://doi.org/10.1103/PhysRevC.52.3151
16. Hagino K., Rowley N., Kruppa A. T. A program for coupled-channel calculations with all order couplings for heavy-ion fusion reactions. *Comp. Phys. Comm.*, 1999, vol. 123, pp. 143–152. https://doi.org/10.1016/S0010-4655(99)00243-X.CCFUL
17. Morton C. R., Berriman A. C., Dasgupta M., Hinde D. J., Newton J. O., Hagino K., Thompson I. J. Coupled-channels analysis of the $^{16}O+^{208}Pb$ fusion barrier distribution. *Phys. Rev.*, 1999, vol. C60, article no. 044608. https://doi.org/10.1103/PhysRevC.60.044608
18. Jisha P., Vinodkumar A. M., Sanila S., Arjun K., Babu B. R. S., Gehlot J., Nath S., Madhavan N., Biswas R., Parihari A., Vinayak A., Mahato A., Prasad E., Visakh A. C. Role of positive transfer Q values in fusion cross sections for $^{18}O+^{182,184,186}W$ reactions. *Phys. Rev.*, 2022, vol. C105, article no. 054614. https://doi.org/10.1103/PhysRevC.105.054614
19. Sun X.-X., Guo L. Microscopic study of compound-nucleus formation in cold-fusion reactions. *Phys. Rev.*, 2022, vol. C105, article no. 054610. https://doi.org/10.1103/PhysRevC.105.054610
20. Błocki J., Randrup J., Świątecк W. J., Tsang C. F. Proximity forces. *Ann. Phys. N. Y.*, 1977, vol. 105, pp. 427–462.
21. Myers W., Świątecki W. Nucleus-nucleus proximity potential and superheavy nuclei. *Phys. Rev.*, 2000, vol. C62, article no. 044610. https://doi.org/10.1103/PhysRevC.62.044610
22. Zagrebaev V. I., Samarin V. V. Near-barrier fusion of heavy nuclei: Coupling of channels. *Phys. At. Nucl.*, 2004, vol. 67, pp. 1462–1477. https://doi.org/10.1134/1.1788037
23. Bansal M., Chopra S., Gupta R. K., Kumar R., Sharma M. K. Dynamical cluster-decay model using various formulations of a proximity potential for compact non-coplanar nuclei: Application to the $^{64}Ni+^{100}Mo$ reaction. *Phys. Rev.*, 2012, vol. C86, article no. 034604. https://doi.org/10.1103/PhysRevC.86.034604
24. Ghodsi O. N., Gharaei R. Analysis of heavy-ion fusion reactions at extreme sub-barrier energies using the proximity formalism. *Phys. Rev.*, 2013, vol. C88, article no. 054617. https://doi.org/10.1103/PhysRevC.88.054617
25. Kühtreiber J., Hille P., Forstner O., Friedmann H., Pavlik A., Priller A. $^{6,7}Li+^{27}Al$ reactions close to and below the Coulomb barrier. *Phys. Rev.*, 2021, vol. C103, article no. 064605. https://doi.org/10.1103/PhysRevC.103.064605
26. Wen P. W., Lin C. J., Jia H. M., Yang L., Yang F., Huang D. H., Luo T. P., Chang C., Zhang M. H., Ma N. R. New Coulomb barrier scaling law with reference to the synthesis of superheavy elements. *Phys. Rev.*, 2022, vol. C105, article no. 034606. https://doi.org/10.1103/PhysRevC.105.034606
27. Gross D. H. E., Kalinowski H. Friction model of heavy-ion collisions. *Phys. Rep.*, 1978, vol. 45, pp. 175–210. https://doi.org/10.1016/0370-1573(78)90031-5
28. Fröbrich P. Fusion and capture of heavy ions above the barrier: Analysis of experimental data with the surface friction model. *Phys. Rep.*, 1984, vol. 116, pp. 337–400. https://doi.org/10.1016/0370-1573(84)90162-5
29. Litnevsky V. L., Pashkevich V. V., Kosenko G. I., Ivanyuk F. A. Description of synthesis of super-heavy elements within the multidimensional stochastic model. *Phys. Rev.*, 2014, vol. C89, article no. 034626. https://doi.org/10.1103/PhysRevC.89.034626
30. Vries H. De, Jager C. W. De, Vries C. De. Nuclear charge-density-distribution parameters from elastic electron scattering. *At. Data Nucl. Data Tables*, 1987, vol. 36, pp. 495–536. https://doi.org/10.1016/0092-640X(87)90013-1
31. Terashima S., Sakaguchi H., Takeda H., Ishikawa T., Itoh M., Kawabata T., Murakami T., Uchida M., Yasuda Y., Yosoi M., Zenihiro J., Yoshida H. P., Noro T., Ishida T., Asaji S., Yonemura T. Proton elastic scattering from tin isotopes at 295 MeV and systematic change of neutron density distributions. *Phys. Rev.*, 2008, vol. C77, pp. 024317. https://doi.org/10.1103/PhysRevC.77.024317
32. Sakaguchi H., Zenihiro J. Proton elastic scattering from stable and unstable nuclei –Extraction of nuclear densities. *Prog. Part. Nucl. Phys.*, 2017, vol. 97, pp. 1–52. https://doi.org/10.1016/0092-640X(87)90013-1
33. Miller G. A. Coherent-nuclear pion photoproduction and neutron radii. *Phys. Rev.*, 2019, vol. C100, article no. 044608. https://doi.org/10.1103/PhysRevC.100.044608
34. Sinha B. The optical potential and nuclear structure. *Phys. Rep.*, 1975, vol. 20, pp. 1–57. https://doi.org/10.1016/0370-1573(75)90011-3
35. Satchler G. R., Love W. G. Folding model potentials from realistic interactions for heavy-ion scattering. *Phys. Rep.*, 1979, vol. 55, pp. 183–254. https://doi.org/10.1016/0370-1573(79)90081-4

36. Bertsch G., Borysowicz J., McManus H., Love W. G. Interactions for inelastic scattering derived from realistic potentials. *Nucl. Phys.*, 1977, vol. A284, pp. 399–419. https://doi.org/10.1016/0375-9474(77)90392-X
37. Anantaraman N., Toki H., Bertsch G. F. An effective interaction for inelastic scattering derived from the Paris potential. *Nucl. Phys.*, 1983, vol. A398, pp. 269–278. https://doi.org/10.1016/0375-9474(83)90487-6
38. Lahiri C., Biswal S. K., Patra S. K. Effects of *NN* potentials on *p* Nuclides in the A ∼100–120 region. *Int. J. Mod. Phys.*, 2016, vol. E25, article no. 1650015. https://doi.org/10.1142/S0218301316500154
39. Bhuyan M., Kumar R. Fusion cross section for Ni-based reactions within the relativistic mean-field formalism. *Phys. Rev.*, 2018, vol. C98, article no. 054610. https://doi.org/10.1103/PhysRevC.98.054610
40. Migdal A. B. *Theory of finite Fermi systems and application to atomic nuclei*. Interscience, New York, 1967. 319 p.
41. Kuzyakin R. A., Sargsyan V. V., Adamian G. G., Antonenko N. V. Quantum Diffusion Description of Large-Amplitude Collective Nuclear Motion. *Phys. Elem. Part. At. Nucl.*, 2017, vol. 48, pp. 21–118.
42. Gontchar I. I., Hinde D. J., Dasgupta M., Newton J. O. Double folding nucleus-nucleus potential applied to heavy-ion fusion reactions. *Phys. Rev.*, 2004, vol. C69, article no. 024610. https://doi.org/10.1103/PhysRevC.69.024610
43. Gontchar I. I., Chushnyakova M. V. A C-code for the double folding interaction potential of two spherical nuclei. *Comp. Phys. Comm.*, 2010, vol. 181, pp. 168–182. https://doi.org/10.1016/j.cpc.2009.09.007
44. Gontchar I. I., Chushnyakova M. V., Sukhareva O. M. Systematic application of the M3Y NN forces for describing the capture process in heavy-ion collisions involving deformed target nuclei. *Phys. Rev.*, 2022, vol. C105, article no. 014612. https://doi.org/10.1103/PhysRevC.105.014612
45. Chushnyakova M. V., Gontchar I. I., Sukhareva O. M., Khmyrova N. A. Modification of the effective Yukawa-type nucleon–nucleon interaction for accelerating calculations of the real part of the optical potential. *Moscow Univ. Phys. Bull.*, 2021, vol. 76, pp. 202–208. https://doi.org/10.3103/S0027134921040056
46. Chien L. H., Khoa D. T., Cuong D. C., Phuc N. H. Consistent mean-field description of the $^{12}C+^{12}C$ optical potential at low energies and the astrophysical *S* factor. *Phys. Rev.*, 2018, vol. C98, article no. 064604. https://doi.org/10.1103/PhysRevC.98.064604
47. Khoa D. T., Knyazkov O. M. Exchange effects in elastic and inelastic alpha- and heavy-ion scattering. *Zeitschrift Für Phys.*, 1987, Bd. A328, S. 67–79. https://doi.org/10.1007/BF01295184
48. Khoa D. T., Satchler G. R., Oertzen W. von. Nuclear incompressibility and density dependent NN interactions in the folding model for nucleus-nucleus potentials. *Phys. Rev.*, 1997, vol. C56, pp. 954–969. https://doi.org/10.1103/PhysRevC.56.954
49. Capote R., Herman M., Obložinský P., Young P. G., Goriely S., Belgya T., Ignatyuk A. V., Koning A. J., Hilaire S., Plujko V. A., Avrigeanu M., Bersillon O., Chadwick M. B., Fukahori T., Ge Z., Han Y., Kailas S., Kopecky J. Maslov V. M., Reffo G., Sin M., Soukhovitskii E. S., Talou P. RIPL – Reference Input Parameter Library for Calculation of Nuclear Reactions and Nuclear Data Evaluations. *Nucl. Data Sheets*, 2009, vol. 110, pp. 3107–3214. https://doi.org/10.1016/J.NDS.2009.10.004
50. Sargsyan V. V., Adamian G. G., Antonenko N. V., Scheid W., Zhang H. Q. Sub-barrier capture with quantum diffusion approach: Actinide-based reactions. *Eur. Phys. J. A.*, 2011, vol. 47, article no. 38. https://doi.org/10.1140/epja/i2011-11038-y
51. Sargsyan V. V., Adamian G. G., Antonenko N. V., Scheid W., Zhang H. Q. Astrophysical *S* factor, logarithmic slope of the excitation function, and barrier distribution. *Phys. Rev. C*, 2012, vol. 86, article no. 034614. https://doi.org/10.1103/PhysRevC.86.034614
52. Chushnyakova M. V., Bhattacharya R., Gontchar I. I. Dynamical calculations of the above-barrier heavy-ion fusion cross sections using Hartree–Fock nuclear densities with the SKX coefficient set. *Phys. Rev. C*, 2014, vol. 90, article no. 017603. https://doi.org/10.1103/PhysRevC.90.017603
53. Gontchar I. I., Chushnyakova M. V. Describing the heavy-ion above-barrier fusion using the bare potentials resulting from Migdal and M3Y double-folding approaches. *J. Phys. G*, 2016, vol. 43, article no. 045111. https://doi.org/10.1088/0954-3899/43/4/045111

Поступила в редакцию 02.01.2023; одобрена после рецензирования 26.01.2023; принята к публикации 03.02.2023
The article was submitted 02.01.2023; approved after reviewing 26.01.2023; accepted for publication 03.02.2023